molecular pharmaceutics

Article

pubs.acs.org/molecularpharmaceutics

Targeted Delivery of Doxorubicin by Folic Acid-Decorated Dual Functional Nanocarrier

Jianqin Lu,[†,‡,§] Wenchen Zhao,[‡] Yixian Huang,[†,‡,§] Hao Liu,[∥] Rebecca Marquez,[∥] Robert B. Gibbs,[‡] Jiang Li,[†,‡,§] Raman Venkataramanan,[‡] Liang Xu,[∥] Shulin Li,[⊥] and Song Li*[,†,‡,§]

[†]Center for Pharmacogenetics, [‡]Department of Pharmaceutical Sciences, School of Pharmacy, and [§]University of Pittsburgh Cancer Institute, University of Pittsburgh, Pittsburgh, Pennsylvania 15261, United States

[∥]Departments of Molecular Biosciences and Radiation Oncology and the University of Kansas Cancer Center, University of Kansas, Lawrence, Kansas 66045, United States

[⊥]Department of Pediatrics Research, University of Texas MD Anderson Cancer Center, Houston, Texas 77030, United States

Supporting Information

ABSTRACT: Doxorubicin (DOX) is one of the most commonly used antineoplastic agents, but its clinical application is oftentimes coupled with severe side effects. Selective delivery of DOX to tumors via nanosized drug carrier represents an attractive approach to this problem. Previously, we developed a dual functional nanomicellar carrier, PEG_{5K}-embelin$_2$ (PEG_{5K}-EB_2), which was able to deliver paclitaxel (PTX) selectively to tumors and to achieve an enhanced therapeutic effect. In the present study, we examined the utility of PEG_{5K}-EB_2 to deliver DOX to tumors. In addition, folic acid (FA) was coupled to the surface of the PEG_{5K}-EB_2 micelles (FA-PEG_{5K}-EB_2) to further improve the selective targetability of the system. DOX-loaded PEG_{5K}-EB_2 micelles were uniformly spherical particles with a diameter of approximately 20 nm. Incorporation of FA had minimal effect on the size of the particles. The DOX loading efficiency was as high as 91.7% and 93.5% for PEG_{5K}-EB_2 and FA-PEG_{5K}-EB_2, respectively. DOX formulated in PEG_{5K}-EB_2 micelles (with or without FA decoration) demonstrated sustained kinetics of DOX release compared to free DOX. FA-PEG_{5K}-EB_2 significantly facilitated the intracellular uptake of DOX over free DOX and PEGylated liposomal DOX (Doxil) in breast cancer cells, 4T1.2, and drug resistant cells, NCI/ADR-RES. P-gp ATPase assay showed that PEG_{5K}-EB_2 significantly inhibited the function of the P-gp efflux pump. The maximum tolerated dose of DOX-loaded PEG_{5K}-EB_2 micelles was 15 mg/kg in mice, which was 1.5-fold greater than that for free DOX. Pharmacokinetics (PK) and biodistribution studies showed that both types of DOX-loaded micelles, especially FA-PEG_{5K}-EB_2, were able to significantly prolong the blood circulation time of DOX and facilitate its preferential accumulation at the tumor tissue. Finally, DOX/PEG_{5K}-EB_2 mixed micelles demonstrated significantly enhanced tumor growth inhibitory effect with minimal toxicity in comparison to free DOX and Doxil and the antitumor activity was further enhanced after the decoration by folic acid. Our data suggest that FA-PEG_{5K}-EB_2 micelles represent a promising DOX delivery system that warrants more study in the future.

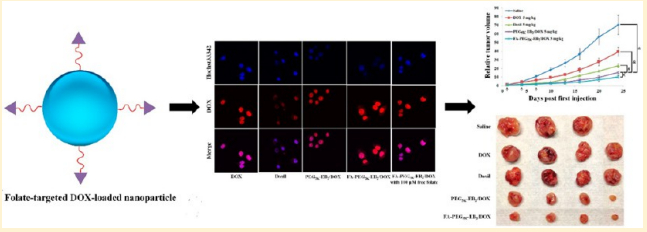

KEYWORDS: *doxorubicin, targeted delivery, folic acid, nanomicelles, multidrug resistance, antitumor activity*

INTRODUCTION

Doxorubicin, an anthracycine antibiotic, is one of the most commonly used anticancer agents for the treatment of various types of cancers, including breast, ovarian, prostate, brain, cervix, and lung cancers. It intercalates between base pairs of the DNA helix, thereby preventing DNA replication and ultimately inhibiting protein synthesis. Additionally, doxorubicin inhibits topoisomerase II, leading to an increased level of stabilized drug−enzyme−DNA cleavable complex during DNA replication and impaired DNA repair. However, the clinical application of DOX has been limited by serious adverse effects.[1,2] Therefore, there is a need for development of strategies to selectively deliver DOX to tumors to improve the therapeutic effect and minimize the untoward toxicity.

Recently, nanomedicine-based platforms have been actively pursued to improve the diagnosis and therapy for a wide range of diseases, including cancer. In order to reduce the adverse effects associated with many antineoplastic agents such as DOX and paclitaxel (PTX), a myriad of nanocarriers have been developed including liposomes, dendrimers, and polymeric micelles. These nanodrug carriers are selectively and passively targeted to tumors through the enhanced permeability and retention effect (EPR).[3,4] In addition, these formulations are capable of evading clearance by the reticuloendothelial system

Received: May 29, 2014
Revised: September 8, 2014
Accepted: September 16, 2014
Published: September 16, 2014

Scheme 1. Synthetic Route of FA-PEG$_{7.5K}$-DOA

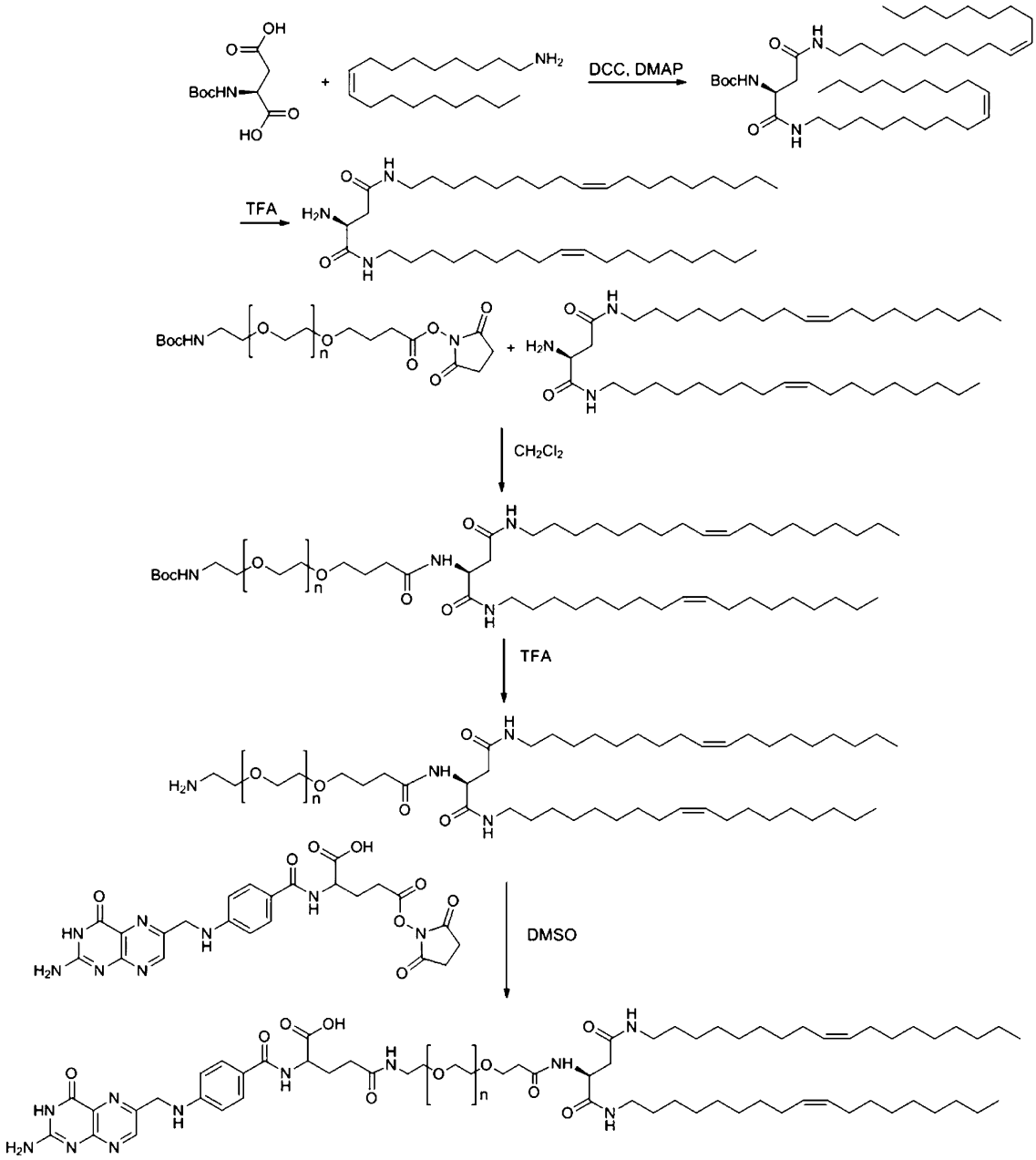

(RES) and thereby circulating in the blood for a prolonged period of time.[5,6] Doxil, PEGylated liposomal DOX, is the first clinically used nanoformulation of DOX approved by the FDA for the treatment of leukemia, breast cancer, lung cancer, brain cancer, and bone cancer. Although the DOX-related toxicity has been reduced to some degree, its anticancer efficacy has been shown to be only marginally improved.[7] Furthermore, Doxil has been shown to cause hand−foot syndrome and mucositis in recent clinical studies.[8−10] Hence, there is need to develop improved formulations for in vivo applications of DOX.

During the past two decades, polymeric micelles have gained considerable attention as an attractive nanomedicine platform due to their technical ease, high biocompatibility, and high biodegradability.[11−16] More importantly, the size of micelles (20−100 nm) is significantly smaller than liposomes (100−200 nm), which renders micelles more effective in passive targeting to solid tumors.[17,18] In addition, a targeting ligand can be introduced into the micellar system to further improve the active targeting to tumors and minimize the nonspecific uptake by normal tissues.[19−22] Different targeting systems have been studied, among which the folate-targeting system has been extensively investigated due to its simplicity and effectiveness.[23−26]

We recently developed a dual functional drug delivery system that is based on PEG-derivatized embelin.[12,13] Embelin is a naturally occurring alkyl substituted hydroxyl benzoquinone compound and a major constituent of *Embelia ribes* BURM. It has been shown that embelin exhibits antitumor activity in various types of cancers via several different mechanisms.[27−31] Embelin is poorly water-soluble and also has limited oral bioavailability.[32] We showed that modification of embelin with PEG led to a significant increase in its water solubility.

dx.doi.org/10.1021/mp500389v | *Mol. Pharmaceutics* 2014, 11, 4164−4178

Interestingly, PEG-embelin self-assembles to form micelles that are capable of delivering other hydrophobic drugs. Delivery of paclitaxel via one such PEG-embelin conjugate, PEG_{5K}-EB_2, led to significantly improved antitumor activity in both breast and prostate cancer models.[13] In this study, we examine the potential application of PEG_{5K}-EB_2 in delivery of DOX. Our data showed that DOX could be effectively formulated in PEG_{5K}-EB_2 micelles. Delivery of DOX via PEG_{5K}-EB_2 micelles led to improved antitumor activity over free DOX or Doxil in vitro and in vivo. In addition, we show for the first time that PEG_{5K}-EB_2 can significantly inhibit the activity of P-gp. Finally, the antitumor activity of DOX-loaded PEG_{5K}-EB_2 micelles was further improved via incorporation of folate.

EXPERIMENTAL SECTION

Materials. Doxorubicin hydrochloride (98%) (DOX·HCl) was purchased from AK Scientific Inc. (CA, U.S.A.). Doxil was purchased from Avanti Polar Lipids (AL, U.S.A.). Boc amine PEG NHS ester (BocNH-PEG-NHS, MW 7500) was purchased from JenKem Technology U.S.A., Inc. (Allen, TX). 2,5-Dihydroxy-3-undecyl-1,4-benzoquinone (embelin, 98%) was purchased from 3B Scientific Corporation (IL, U.S.A.). Folic acid NHS ester, methoxy-$PEG_{5,000}$-OH, dimethyl sulfoxide (DMSO), 3-(4,5-dimethylthiazol-2-yl)-2,5-diphenyl tetrazolium bromide (MTT), aspartic acid, trypsin-EDTA solution, Triton X-100, and Dulbecco's Modified Eagle's Medium (DMEM) were all purchased from Sigma-Aldrich (MO, U.S.A.). Fetal bovine serum (FBS) and penicillin–streptomycin solution were from Invitrogen (NY, U.S.A.). RPMI-1640 medium was purchased from Life Technologies (NY, U.S.A.). All solvents used in this study were HPLC grade.

Synthesis of PEG_{5K}-EB_2. PEG_{5K}-EB_2 was synthesized according to the methods described previously.[12,13] Briefly, benzoquinone was first synthesized followed by coupling to Boc-aspartic acid. Then, undecyl side chains were conjugated to each of the two benzoquinone rings to form aspartic acid-EB_2. Finally, methoxy-PEG_{5K}-OH was coupled to aspartic acid-EB_2 to generate PEG_{5K}-EB_2 via the deprotected amino group. The final product was analyzed by ^{1}NMR and MALDI–TOF.

Synthesis of Folic Acid-$PEG_{7.5K}$-DOA (Dioleyl Amido Aspartic Acid). Folate-$PEG_{7.5K}$-DOA was constructed based on the method reported by Zhang et el. with slight modification.[33] Briefly, Boc-aspartic acid was linked to oleyl amine in the presence of DCC and DMAP in anhydrous CH_2Cl_2. After the reaction was completed, the mixture was filtered and evaporated under reduced pressure, and the residue was purified by flash column chromatography to obtain Boc-dioleyl amine (Boc-DOA). Then, trifluoroacetic acid (TFA) was added to remove Boc group in Boc-DOA to expose the active NH_2 followed by reaction with BocNH-$PEG_{7.5K}$-NHS to form BocNH-$PEG_{7.5K}$-DOA. After purification via precipitation with cold diethyl ether and ethanol, Boc group in BocNH-$PEG_{7.5K}$-DOA was removed by TFA. Finally, NH_2-$PEG_{7.5K}$-DOA was reacted with folic acid (FA) NHS ester to yield FA-$PEG_{7.5K}$-DOA. The compete synthesis route was illustrated in Scheme 1.

Preparation and Physiochemical Characterization of DOX-Loaded PEG_{5K}-EB_2 and FA- PEG_{5K}-EB_2 Micelles. DOX·HCl was first neutralized by 3 mol equiv of triethylamine in $CHCl_3$/MeOH (1:1. v:v) to remove HCl from the parent compound. DOX-loaded PEG_{5K}-EB_2 was prepared as reported previously.[13] Briefly, DOX (10 mM in $CHCl_3$/MeOH) was added to PEG_{5K}-EB_2 (10 mM in chloroform) with different carrier/drug molar ratios. The organic solvent was first removed by nitrogen flow to form a thin dry film of drug/carrier mixture. The dry film was further dried under high vacuum for 2 h to remove any traces of remaining solvent. The film was then reconstituted in saline without further sonication. The FA-PEG_{5K}-EB_2 was composed of PEG_{5K}-EB_2/FA-$PEG_{7.5K}$-DOA at molar ratios of 99.5:0.5 according to the literature.[26] The DOX-formulated FA-PEG_{5K}-EB_2 micelles were prepared similarly as mentioned above. The mean diameter, size distribution, and zeta potential of micelles with or without loaded drug were evaluated by dynamic light scattering (DLS). The morphology of DOX-free or loaded micelles was observed under TEM. The concentration of DOX in DOX-loaded micelles was examined by HPLC with the detector set at 233 nm. The drug loading capacity (DLC) and drug loading efficiency (DLE) were calculated according to the following formula:

$$\mathrm{DLC}(\%) = \frac{\text{weight of drug used}}{(\text{weight of polymer} + \text{drug used})} \times 100\%$$

$$\mathrm{DLE}(\%) = \frac{\text{weight of loaded drug}}{\text{weight of input drug}} \times 100\%$$

Release Kinetics of DOX Formulated in Micelles. The in vitro release kinetics of DOX was carried out by dialysis method using DPBS (pH = 7.4) containing 0.5% (w/v) Tween 80 as the release medium. Free DOX was employed as a control. A total of 2 mL of DOX-loaded PEG_{5K}-EB_2 or FA-PEG_{5K}-EB_2 micelles (1 mg DOX/mL) were sealed in dialysis tubes (MWCO = 12 kDa, Spectrum Laboratories). The dialysis tubes were immersed in 500 mL release medium in a beaker covered with Parafilm. The beakers were kept in an incubator shaker at 100 rpm and 37 °C. At different time points, the concentration of DOX retained in the dialysis tubes was measured by HPLC with the detector set at 233 nm. Values were reported as the means from triplicate samples.

Cell Culture. Mouse breast cancer cell line, 4T1.2, human breast cancer cell line, MCF-7, and drug-resistant cancer cell line, NCI/ADR-RES, were used in this study. All cell lines were cultured in RPMI-1640 medium (NY.U.S.A.) containing 10% fetal bovine serum (FBS) and 1% penicillin–streptomycin in a humidified incubator at 37 °C with 5% CO_2.

Animals. Female BALB/c mice, 8–10 weeks, were purchased from Charles River (Davis, CA, U.S.A.). All animals were housed under pathogen-free conditions according to AAALAC (Association for Assessment and Accreditation of Laboratory Animal Care) guidelines. All animal-related experiments were performed in full compliance with institutional guidelines and approved by the Animal Use and Care Administrative Advisory Committee at the University of Pittsburgh.

In Vitro Cytotoxicity Assay. The cytotoxicity of DOX formulated in micelles was assessed in different cancer cell lines (4T1.2, MCF-7, and NCI/ADR-RES) and compared to free DOX and Doxil. Briefly, cells were seeded in 96-well plates followed by 24 h incubation in RPMI-1640 medium with 10% FBS and 1% streptomycin–penicillin. Different DOX formulations with varying concentrations (at the equivalent concentrations of DOX) were added to cells. Controls including PEG_{5K}-EB_2 and FA-PEG_{5K}-EB_2 were added to cells at concentrations equivalent to those of carriers in the corresponding DOX formulation groups. In order to confirm

the active targeting effect rendered by folate ligand attached to the PEG_{5K}-EB_2 micelles, free folate (100 μM), as a competitive inhibitor to folate receptor, was added along with the FA-PEG_{5K}-EB_2/DOX micelles.[34] Cells were incubated for 72 h and cell viability was assessed by MTT assay as described previously.[12,13]

Intracellular Uptake Study. A total of 3×10^5 4T1.2 and NCI/ADR-RES cells were seeded into each well of 6-well plates and were allowed to grow overnight. Then the medium was replaced by fresh medium containing free DOX, Doxil, and DOX-loaded PEG_{5K}-EB_2 and FA-PEG_{5K}-EB_2 micelles, respectively, at an equivalent DOX concentration of 6 μg/mL. Following incubation for 30 min at 37 °C, the cells were washed three times with cold PBS and fixed with 4% paraformaldehyde for 30 min. Afterward, the nuclei were stained by Hoechst33342 for 5 min. Subsequently, cells were washed three times with cold saline. Finally, the intracellular uptake of DOX in various formulations was observed under confocal laser scanning microscopy (CLSM, FluoView 1000, Olympus, Japan).

Quantitative cellular uptake of various DOX formulations was evaluated by flow cytometry. Briefly, 4T1.2 and NCI/ADR-RES cells were seeded into the 6-well plates at a density of 3×10^5 cells/well. After overnight attachment, cells were treated with free DOX, Doxil, DOX-loaded PEG_{5K}-EB_2 and FA-PEG_{5K}-EB_2, and DOX-formulated in FA-PEG_{5K}-EB_2 micelles along with 100 μM free folic acid, respectively, at an equivalent DOX concentration of 6 μg/mL. Cells without treatment were used as a control. Following incubation at 37 °C for 30 min, cells were washed with cold PBS three times and resuspended in 500 μL PBS for the flow cytometry analysis with CyAn ADP Analyzer (Beckman Coulter, Inc.). Cell-associated DOX was excited with an argon laser (480 nm), and fluorescence was detected at 570 nm. A total of 20 000 events were collected for each sample.

P-gp ATPase Assay. The effect of PEG_{5K}-EB_2 conjugate on P-gp was studied via examining its effect on a verapamil-stimulated ATPase activity as reported previously.[14] TPGS was included as a positive control and sodium orthovanadate (Na_3VO_4) was used as a selective inhibitor of P-gp. Briefly, test samples containing verapamil (50 μM) along with PEG_{5K}-EB_2 or TPGS (10 μM and 100 μM) or Na_3VO_4 were added to 96-well plates and incubated with P-gp membrane for 5 min at 37 °C. Then, the reaction was initiated by the addition of MgATP followed by another 40 min incubation at 37 °C. The samples were then removed from 37 °C incubator and ATP detection reagent was added in order to develop the luminescence. Signals were measured 20 min later on a microplate luminometer (Victor^2 1420 multilabel counter). The changes of relative light unit (ΔRLU) were calculated as follows:

$$\Delta\text{RLU} = (\text{luminescence of } Na_3VO_4\text{-treated group}) - (\text{luminescence of the samples treated by the mixture of verapamil and } PEG_{5K}\text{-}EB_2 \text{ or TPGS conjugate})$$

Maximum Tolerated Dose (MTD). Groups of 3 female BALB/c mice were treated intravenously with free DOX (5, 10, 15 mg DOX/kg body weight) or DOX-loaded PEG_{5K}-EB_2 micelles (5, 10, 15, 20, 30 mg DOX/kg body weight), respectively. Changes in body weight and survival of mice were followed daily for 2 weeks. The MTD was defined as the maximal dose that causes neither mouse mortality owing to the systemic toxicity nor greater than 15% loss in body weight as well as other noticeable changes in the general movement and signs within the entire period of the experiments.

In Vivo Near-Infrared Fluorescence (NIRF) Optical Imaging. The in vivo tumor-targeting efficiency and biodistribution of PEG_{5K}-EB_2 micelles were studied by using a near-infrared fluorescence dye, DiR. Two CL1 tumor-bearing nude mice were employed in this experiment. Briefly, 200 μL of DiR-loaded PEG_{5K}-EB_2 micelles (10 nmol DiR) was iv injected into one mouse and another mouse (as a control) was iv injected with 200 μL of DiR in ethanol/water (1:4 v/v) solution. At different time points (4 h, 24 h, 48 h, 72 h, and 96 h) postinjection, mice were scanned using a Carestream Molecular Imaging System (Carestream Health, Inc.) with excitation at 750 nm and emission at 780 nm using an exposure time of 60 s. After 96 h, mice were euthanized by CO_2 overdose. Tumors and major organs of mice were excised and imaged with Carestream Molecular Imaging System. The tissue distribution of DiR in tumors and other organs were quantified by measuring the signal intensity at the region of interest.

Pharmacokinetics and Biodistribution of DOX in Vivo. Free DOX and DOX-loaded micelles were administered via the tail vein with a dosage of 5 mg of DOX/kg in 200 μL saline (n = 3). At predetermined time points (3 min, 8 min, 15 min, 30 min, 45 min, 1 h, 2 h, 4 h, 8 h, and 12 h), blood samples were obtained from mice using a heparinized capillary tube. Plasma samples were isolated from the blood by centrifuging at 3000 rpm for 10 min. DOX in plasma was extracted by extraction buffer (10% Triton X-100, deionized water, and isopropanol at volumetric ratio of 1:2:15). The concentration of DOX at different time points was measured by HPLC with the detector set at 233 nm (Waters Alliance 2695 Separations Module combined with Waters 2998 Photodiode Array Detector; Waters Symmetry C18 5 μm 4.6 × 250 mm column; mobile phase, 80% MeOH:20% H_2O isocrate; flow rate, 0.6 mL/min). Pharmacokinetic parameters such as $t_{1/2}$, area under the curve (AUC), volume of distribution (V_d), and clearance (CL) were calculated by fitting the blood DOX concentrations to a noncompartment model using Phoenix WinNonlin.

In biodistribution study, free DOX, DOX-loaded PEG_{5K}-EB_2, and DOX-loaded FA-PEG_{5K}-EB_2 micelles were intravenously injected into 4T1.2 tumor bearing mice at the dose of 5 mg of DOX/kg, respectively (n = 3). At 24 h postinjection, tumor tissues, major organs (liver, spleen, lung, heart, and kidney) and blood were harvested from the mice. Tissues were homogenized using Power Gen 500 homogenizer (Fisher Scientific) with 100 mg of tissues mixed with 900 μL of extraction buffer, and DOX was extracted overnight at −20 °C using the same method mentioned above. The samples were centrifuged at 3000 rpm for 10 min, and the supernatant was then dried and dissolved in 400 μL of 75% MeOH. Afterward, the sample solutions were subjected to further centrifugation at 14 500 rpm for 5 min to remove undissolved materials prior to HPLC measurement mentioned above. The percent injected dose and the percent injected dose per gram (tissue) values were calculated using the following equations:

Table 1. Physicochemical Characterization of Blank and DOX-Loaded Micelles

micelles	molar ratios	size (nm)	PDI	zeta potential (mv)	DLC (%)	DLE (%)
PEG_{5k}-EB_2		20.6 ± 0.1	0.05	0.68 ± 0.13		
PEG_{5k}-EB_2:DOX	2:1	23.1 ± 0.6	0.12	0.98 ± 0.21	4.55	91.7
FA-PEG_{5k}-EB_2		21.3 ± 0.5	0.09	−0.39 ± 0.09		
FA-PEG_{5k}-EB_2:DOX	2:1	24.9 ± 1.2	0.11	0.46 ± 0.16	4.52	93.5

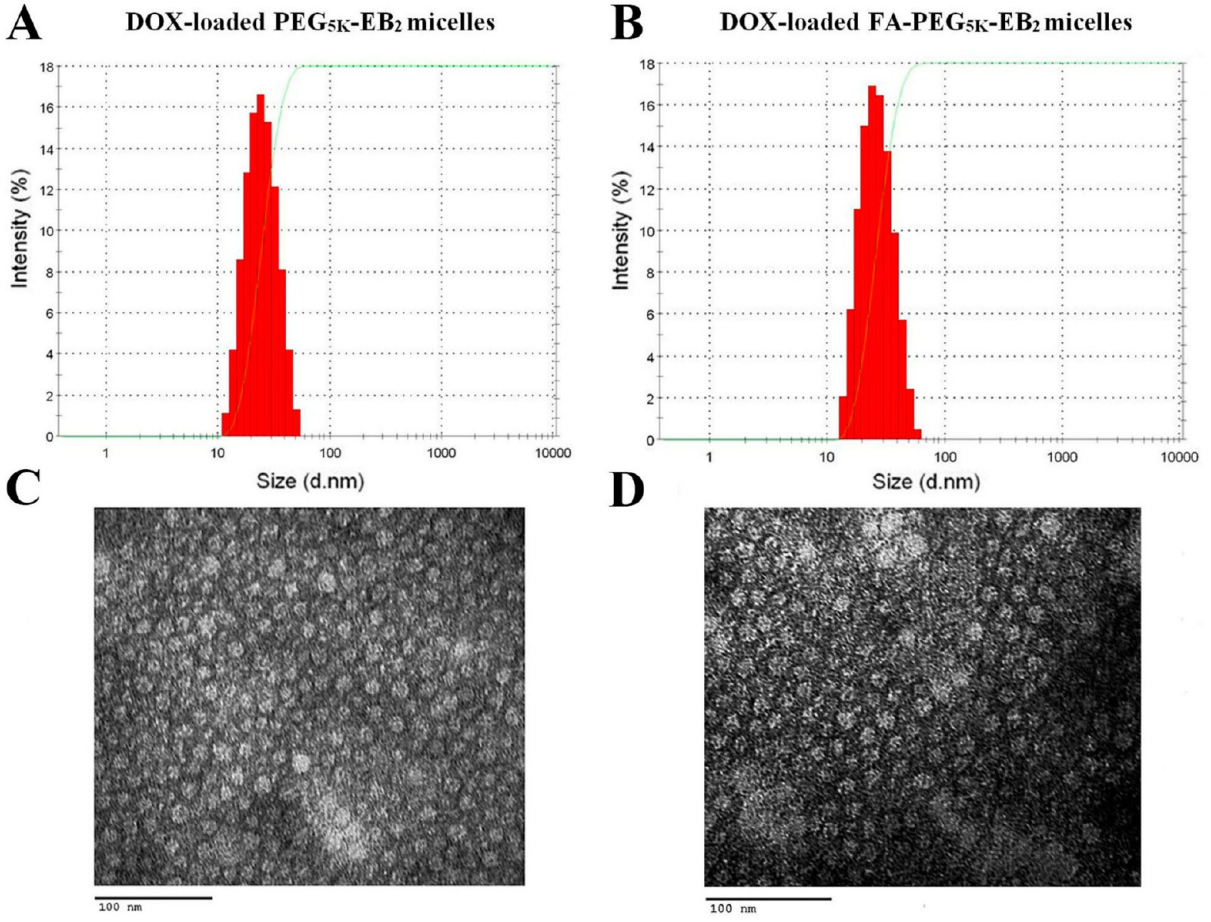

Figure 1. Characteristics of DOX-loaded nanoassemblies. Size distribution of PEG_{5K}-EB_2/DOX micelles (A) and FA-PEG_{5K}-EB_2/DOX micelles (B) measured by dynamic light scattering (DLS). Transmission electron microscopic (TEM) images of PEG_{5K}-EB_2/DOX micelles (C) and FA-PEG_{5K}-EB_2/DOX micelles (D). DOX concentration was kept at 1 mg/mL.

$$\%\ \text{injected dose} = \frac{\text{dose in blood or in tissue samples}}{\text{injected dose}} \times 100\%$$

$$\frac{\%\ \text{injected dose}}{\text{g tissue}} = \frac{\%\ \text{injected dose}}{\text{weight of tissue (g)}}$$

In Vivo Antitumor Therapeutic Study. A syngeneic murine breast cancer model (4T1.2) was used to evaluate the therapeutic efficacy of different DOX formulations. Briefly, 2×10^5 4T1.2 cells in 200 μL and saline were inoculated subcutaneously at the right flank of female BALB/c mice. When tumors in the mice reached a volume of 50−100 mm^3, mice were randomly assigned to one of five groups ($n = 5$) and this day was designated as day 1. From day 1, mice were intravenously administered free DOX (5 mg/kg), Doxil (5 mg/kg), DOX-loaded PEG_{5K}-EB_2 or DOX-loaded FA-PEG_{5K}-EB_2 once every 3 days on days 1, 4, and 7, respectively. Tumor sizes were measured with a digital caliper on days 1, 4, 7, 10, 13, 16, 20, 24 and calculated according to the following formula: ($L \times W^2$)/2, where L and W are length and width of each tumor. To better compare between groups, relative tumor volume (RTV) was calculated at each measurement time point, where RTV = the tumor volume at a given time point/the tumor volume prior to first treatment. The tumor growth inhibition rate (IR) was assessed and defined as IR % = (1 − relative tumor volume in the treated group/relative tumor volume in the saline group) × 100%. Toxicity also was monitored by following the body weights of all mice throughout the entire experiment. Mice were sacrificed when tumor reached 2000 mm^3 or developed ulceration. In addition, blood samples were collected from all mice at the completion of the study for the measurement of serum chemistry including aspartate aminotransferase (AST) and alanine aminotransferase (ALT).

Statistical Analysis. In all statistical analyses, the significance level was set at a probability of $P < 0.05$. All results were reported as the mean ± standard deviation (SD) unless otherwise indicated. Statistical analysis was performed by using the Student's t test for two groups, and one-way ANOVA

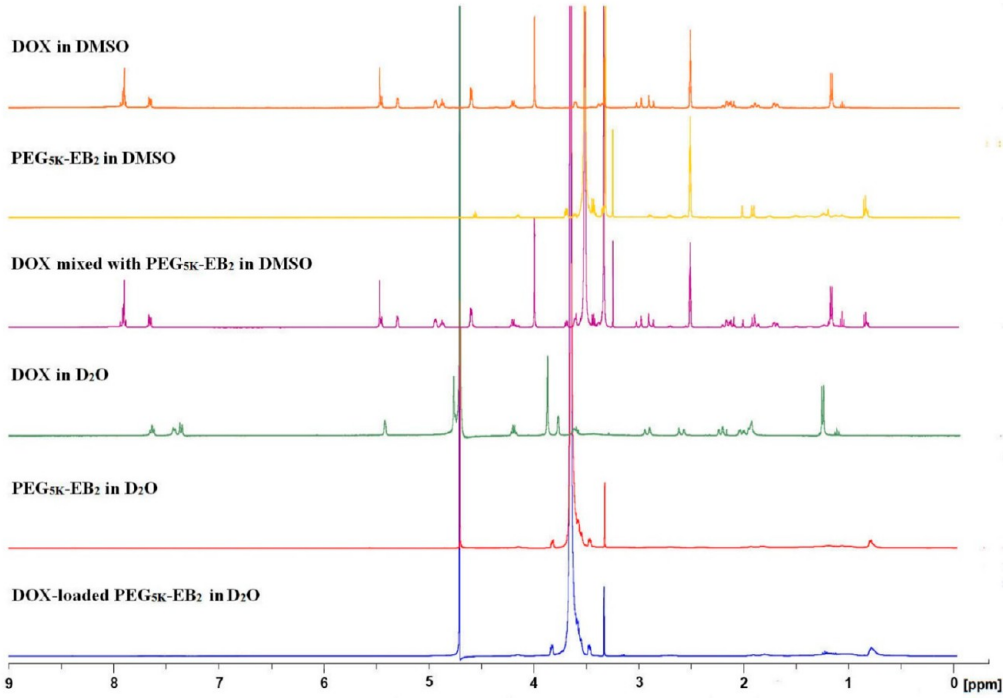

Figure 2. ^{1}NMR spectra of free DOX in D_2O, PEG_{5K}-EB_2 in D_2O or $CDCl_3$ and DOX-formulated in PEG_{5K}-EB_2 micelles in D_2O. Concentration of DOX was 1 mg/mL.

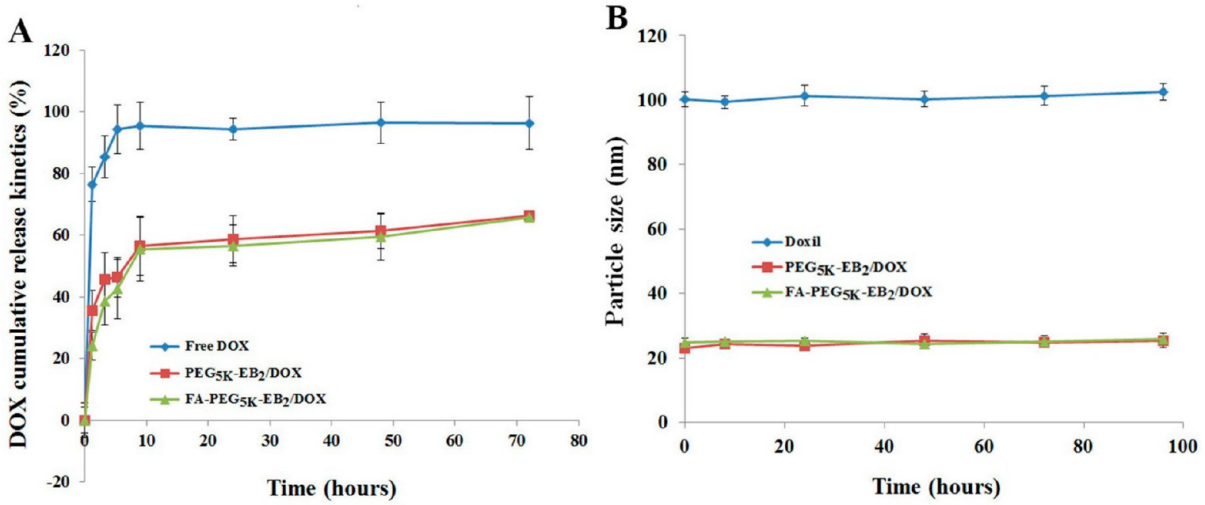

Figure 3. (A) Cumulative release kinetics of DOX from free DOX and DOX-loaded micelles determined by dialysis against DPBS (pH = 7.4) containing 0.5% (w/v) Tween 80. (B) Particle size change of DOX-loaded micelles and Doxil measured by DLS in aqueous solution over time at 37 °C. DOX concentration was kept at 1 mg/mL.

for multiple groups, followed by Newman−Keuls test if $P < 0.05$.

RESULTS AND DISCUSSION

Synthesis and Characterization of FA-$PEG_{7.5K}$-DOA and PEG_{5K}-EB_2. PEG_{5K}-EB_2 was synthesized and characterized as previously reported.[12,13] FA-$PEG_{7.5K}$-DOA was also synthesized to mediate active targeted delivery of PEG_{5K}-EB_2 micelles to tumor cells that overexpress folate receptor (FR). A PEG of longer length ($PEG_{7.5K}$) was used as a spacer between FA and the lipid anchor (DOA) to improve the accessibility of FA on the surface of FA-decorated PEG_{5K}-EB_2 micelles for interaction with FR-overexpressing tumor cells. FA-$PEG_{7.5K}$-DOA conjugate was synthesized via stepwise solution-phase condensation reactions using BocNH-$PEG_{7.5K}$-NHS, Boc-aspartic acid, oleyl amine and FA NHS as building blocks. The complete synthetic route is described in Scheme 1. FA-$PEG_{7.5K}$-DOA was 95.03% pure as verified by HPLC (Supporting Information Figure S1). ^{1}H NMR spectrum of FA-$PEG_{7.5K}$-DOA showed signals at 6.65, 7.65, and 8.65 ppm which are a typical spectrum of FA (Supporting Information Figure S2). MALDI−TOF further confirmed the identity of the compound (Supporting Information Figure S3). These data suggest successful synthesis of FA-$PEG_{7.5K}$-DOA conjugate.

Physicochemical Characterization of DOX-Free and DOX-Loaded Micelles. In aqueous solution, both PEG_{5K}-EB_2

dx.doi.org/10.1021/mp500389v | Mol. Pharmaceutics 2014, 11, 4164−4178

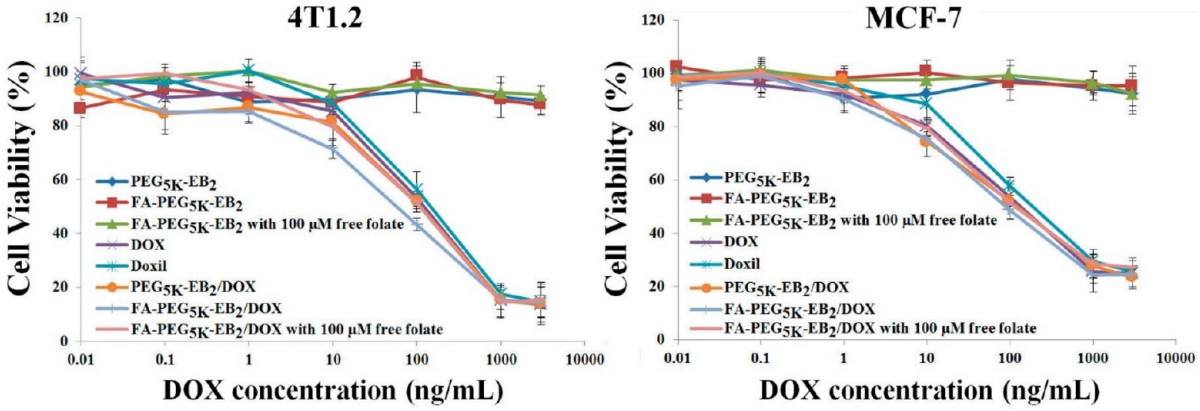

Figure 4. Cytotoxicity of DOX-loaded PEG_{5K}-EB_2 and FA-PEG_{5K}-EB_2 micelles against a mouse breast cancer cell line 4T1.2 and human breast cancer cell line-MCF-7 in comparison to DOX and Doxil. Cells were treated with indicated concentrations of different DOX formulations for 72 h, and cytotoxicity was then evaluated by MTT assay. Values reported are the mean ± SD for triplicate samples.

and FA-PEG_{5K}-EB_2 were able to readily self-assemble to form nanomicelles with a particle diameter around 20 nm as measured by DLS analysis (Table 1). Figure 1A shows the size distribution of PEG_{5K}-EB_2 micelles following incorporation of DOX (1 mg/mL). The size of DOX-loaded micelles was similar to that of drug-free micelles. In addition, spherical particles of uniform size were observed under TEM (Figure 1C). The sizes of the particles under TEM were consistent with those determined by DLS (Figure 1A). It is also apparent that attachment of FA to the surface of the micelles had no impact on their size and morphology (Figure 1B and D).

Table 1 shows that a DOX loading efficiency (DLE) of 91.7 and 93.5% was achieved for PEG_{5K}-EB_2 and FA-PEG_{5K}-EB_2 micelles, respectively, at a carrier/drug molar ratio of 2/1. To confirm that DOX was indeed incorporated into the interior hydrophobic core of PEG_{5K}-EB_2 micelles, we examined the ^1H NMR spectrum of DOX/PEG_{5K}-EB_2 in DMSO and deuterium oxide (D_2O), respectively. As shown in Figure 2, free DOX showed a ^1H NMR spectrum in D_2O that was consistent with previous reports.[35] A similar spectrum was collected when DOX was examined in DMSO. PEG_{5K}-EB_2 in DMSO exhibited a ^1H NMR spectrum that was consistent with its structure (Figure 2). The signals for both DOX and PEG_{5K}-EB_2 were clearly visualized when DOX/PEG_{5K}-EB_2 was examined in DMSO (Figure 2). However, when the ^1H NMR spectrum of PEG_{5K}-EB_2 was collected in D_2O, the embelin signals (0.5−3 ppm, 4−5 ppm) were nearly abolished (Figure 2). This is consistent with the notion that embelin molecules were tightly packed in the core of the micelles in aqueous solution and that embelin signals were shielded by PEG. A similar shielding of embelin signals was observed when DOX/PEG_{5K}-EB_2 was examined in D_2O. The typical peaks for DOX also were completely suppressed for DOX/PEG_{5K}-EB_2, suggesting that DOX was effectively incorporated into the interior core of DOX/PEG_{5K}-EB_2 micelles. A number of mechanisms are likely to be involved in the drug (DOX)/carrier (embelin) interactions including $\pi-\pi$ stacking, hydrogen bonding, as well as hydrophobic/hydrophobic interactions.

Release Kinetics of DOX Formulated in Micelles. The release profile of DOX formulated in PEG_{5K}-EB_2 and FA-PEG_{5K}-EB_2 micelles was evaluated using dialysis method in PBS (pH = 7.4) to simulate physiologically relevant conditions. Free DOX was employed as a control. As depicted in Figure 3, DOX formulated in PEG_{5K}-EB_2 micelles exhibited sustained release kinetics in comparison to free DOX. During the first 9 h, the amount of DOX released in the free DOX group reached 95.35%, which was substantially higher than that in PEG_{5K}-EB_2 micelles (57.45%). Strikingly, no initial burst release of DOX was observed for DOX-loaded PEG_{5K}-EB_2 micelles, indicating that an overall strong force was involved in the drug-carrier interaction. Additionally, DOX formulated in PEG_{5K}-EB_2 micelles displayed a much slower DOX release compared to free DOX during the entire experimental period. The $T_{1/2}$ of DOX release was 55.87 h for DOX/PEG_{5K}-EB_2 mixed micelles, which is significantly longer than that for free DOX (0.82 h). The significantly slower and controlled release in DOX-loaded PEG_{5K}-EB_2 micellar formulation may be attributed to the strong $\pi-\pi$ stacking, hydrogen bonding, as well as hydrophobic interaction between the carrier and DOX as embelin has a benzoquinone ring and a long alkyl chain. Decoration of PEG_{5K}-EB_2 micelles with FA had negligible impact with respect to the DOX release kinetics (Figure 3).

In Vitro Cytotoxicity on Cancer Cells. Figure 4 shows the antiproliferative effect of various DOX formulations on 4T1.2 mouse breast cancer cells. Cells were treated with different DOX formulations and the cytotoxicity was measured by MTT assay 72 h later. All of the DOX formulations showed time- and concentration-dependent cell-killing effect on 4T1.2 cells. As summarized in Table 2, The IC_{50} was 176.13, 248.98, 138.93, and 78.53 ng/mL for DOX, Doxil, PEG_{5K}-EB_2/DOX, and FA-PEG_{5K}-EB_2/DOX micelles, respectively. DOX-loaded FA-PEG_{5K}-EB_2 is the most potent among all the DOX formulations with respect to cell growth inhibition. To determine whether this is due to folate-mediated active targeting, free folate (100 μM) was coadded to cells with the DOX-loaded FA-PEG_{5K}-EB_2 micelles. It has been reported that 100 μM free folate can block more than 99% of the binding by folate receptor.[34] Indeed, the

Table 2. IC_{50} of Different DOX Formulations in 4T1.2 and MCF-7 Cancer Cells

	IC_{50} (ng/mL)				
	DOX	Doxil	PEG_{5K}-EB_2/DOX	FA-PEG_{5K}-EB_2/DOX	FA-PEG_{5K}-EB_2/DOX with 100 μM free folate
4T1.2	176.13	248.98	138.93	78.53	130.13
MCF-7	211.53	345.16	173.19	95.18	148.76

dx.doi.org/10.1021/mp500389v | Mol. Pharmaceutics 2014, 11, 4164−4178

presence of excess free folate decreased the cytotoxicity of DOX-loaded FA-PEG_{5K}-EB_2 micelles to a level that was comparable to that for DOX-loaded PEG_{5K}-EB_2, suggesting that the greater in vitro cytotoxicity of DOX-loaded FA-PEG_{5K}-EB_2 micelles was attributed to the specific ligand−receptor interaction. On the other hand, the relatively high IC_{50} of Doxil might be ascribed to the insufficient intracellular internalization as confirmed in the later uptake study. The inadequate release of DOX from Doxil inside cells may also play a role. Similar results were obtained in MCF-7 human breast cancer cell line (Figure 4).

After demonstrating effective inhibition of proliferation of 4T1.2 and MCF-7 cells, we further studied the cytotoxicity of PEG_{5K}-EB_2/DOX in a drug-resistant cell line, NCI/ADR-RES. Drug resistance is a major factor involved in the failure of many types of cancer chemotherapy.[36] Various mechanisms have been identified that are involved in the different types and/or stages of cancers.[37,38] One primary mechanism involves the overexpression of P-glycoprotein (P-gp), which plays a vital role in the development of multiple drug resistance (MDR).[39−43] P-gp, a member of ATP-binding cassette transporter, is one of the major drug efflux transporters and increased expression of P-gp leads to decreased drug accumulation in multidrug-resistant cells and the development of resistance to anticancer drugs.[44] NCI/ADR-RES is one such MDR cell line and was extensively used for the investigation of multidrug resistance. As shown in Figure 5, the antiproliferative

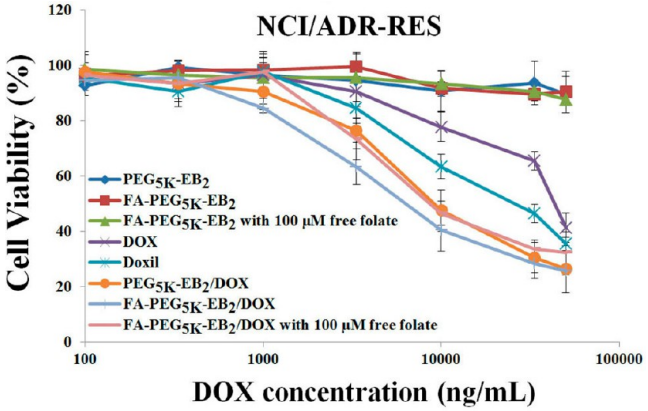

Figure 5. To investigate whether DOX-loaded PEG_{5K}-EB_2 micelles can reverse the multidrug resistance, cytotoxicity was evaluated in NCI/ADR-RES cells. Cells were treated with DOX, Doxil, and DOX-loaded PEG_{5K}-EB_2 and FA-PEG_{5K}-EB_2 micelles for 72 h with various concentrations and then cytotoxicity was determined by MTT assay. Values reported are the mean ± SD for triplicate samples.

effect of all of the DOX formulations was decreased significantly in this cell line. This is likely due to the increased P-gp activity and, therefore, decreased DOX accumulation in NCI/ADR-RES cells, which was confirmed in later DOX cellular uptake studies. In addition, unlike in 4T1.2 and MCF-7 cells, Doxil was more potent than free DOX in inhibiting the proliferation of NCI/ADR-RES cells. This is likely ascribed to an altered route of cellular uptake of Doxil, which decreases the availability of intracellularly delivered DOX to P-gp. These data are consistent with the previous work by Ogawara et al.[45] It is also apparent from Figure 5 that DOX-loaded PEG_{5K}-EB_2 micelles exhibited enhanced antiproliferative effect over DOX and Doxil in NCI/ADR-RES cells, with an improvement of efficacy by 3.67- and 2.02-folds, respectively (Table 3). In addition, coupling of folate to PEG_{5K}-EB_2/DOX micelles led to

Table 3. IC_{50} of Varied DOX Formulations in NCI/ADR-RES Cancer Cell

	IC_{50} (μg/mL)				
	DOX	Doxil	PEG_{5K}-EB_2/DOX	FA-PEG_{5K}-EB_2/DOX	FA-PEG_{5K}-EB_2/DOX with 100 μM free folate
NCI/ADR-RES	43.97	28.43	9.42	7.19	9.11

further improvement in the cytotoxicity toward NCI/ADR-RES cells (Figure 5). Again, addition of free folate was able to reverse the improvement via inhibiting the specific binding of folate receptor to DOX-loaded FA-PEG_{5K}-EB_2 micelles.

In Vitro Cellular Uptake. To investigate whether the enhanced cytotoxicity of our micellar systems was attributed to the improved intracellular DOX accumulation, the cellular uptake of DOX in different formulations was examined in 4T1.2 cells using confocal laser scanning microscopy (CLSM). Figure 6A shows the intracellular distribution of DOX at 30 min following treatment with different DOX formulations. DOX fluorescence signal was largely localized in the nucleus, suggesting that DOX was effectively translocated into the nucleus following delivery into the cytoplasm. It is also apparent that less fluorescence intensity was observed inside the cells treated with Doxil compared with all other formulations.

To better investigate the uptake efficiency, the intracellular accumulation of DOX was further examined quantitatively by flow cytometry. Figure 7A shows the data generated from 4T1.2 cells. In agreement with the confocal study, cells treated with Doxil showed the lowest mean fluorescence intensity. The level of cell-associated fluorescence intensity for PEG_{5K}-EB_2/DOX mixed micelles was similar to that for free DOX. However, surface decoration of PEG_{5K}-EB_2/DOX mixed micelles by FA significantly enhanced the intracellular DOX accumulation over free DOX and Doxil. The improvement in uptake of DOX-loaded FA-PEG_{5K}-EB_2 micelles was significantly abolished in the presence of excess free folate. These data, again, support the notion that the enhanced cellular uptake of DOX-loaded FA-PEG_{5K}-EB_2 micelles was specifically mediated by the folate receptor that is overexpressed on the tumor cells. We also examined the DOX uptake in NCI/ADR-RES cells treated with different DOX formulations (Figure 6B). Overall, the fluorescence signals were significantly weaker for all of the DOX formulations compared to the data generated from 4T1.2 cells (Figure 6A). In addition, most of the fluorescence signals were localized outside of the nucleus. This is consistent with the notion that P-gp activity is significantly increased in NCI/ADR-RES cells and significant amounts of "freely accessible" cytoplasmic DOX are effluxed out of the cells. It is also apparent that NCI/ADR-RES cells treated with free DOX showed lowest level of fluorescence signals compared to cells treated with other formulations (Figure 6B). Figure 7B shows the data of flow cytometry generated from NCI/ADR-RES cells. The data were consistent with confocal imaging. Cells treated with FA-PEG_{5K}-EB_2/DOX micelles gave the highest level of fluorescence intensity. Again, unlike the data generated from the drug-sensitive cells (Figure 7A), Doxil-treated-NCI/ADR-RES cells showed significantly higher levels

dx.doi.org/10.1021/mp500389v | Mol. Pharmaceutics 2014, 11, 4164−4178

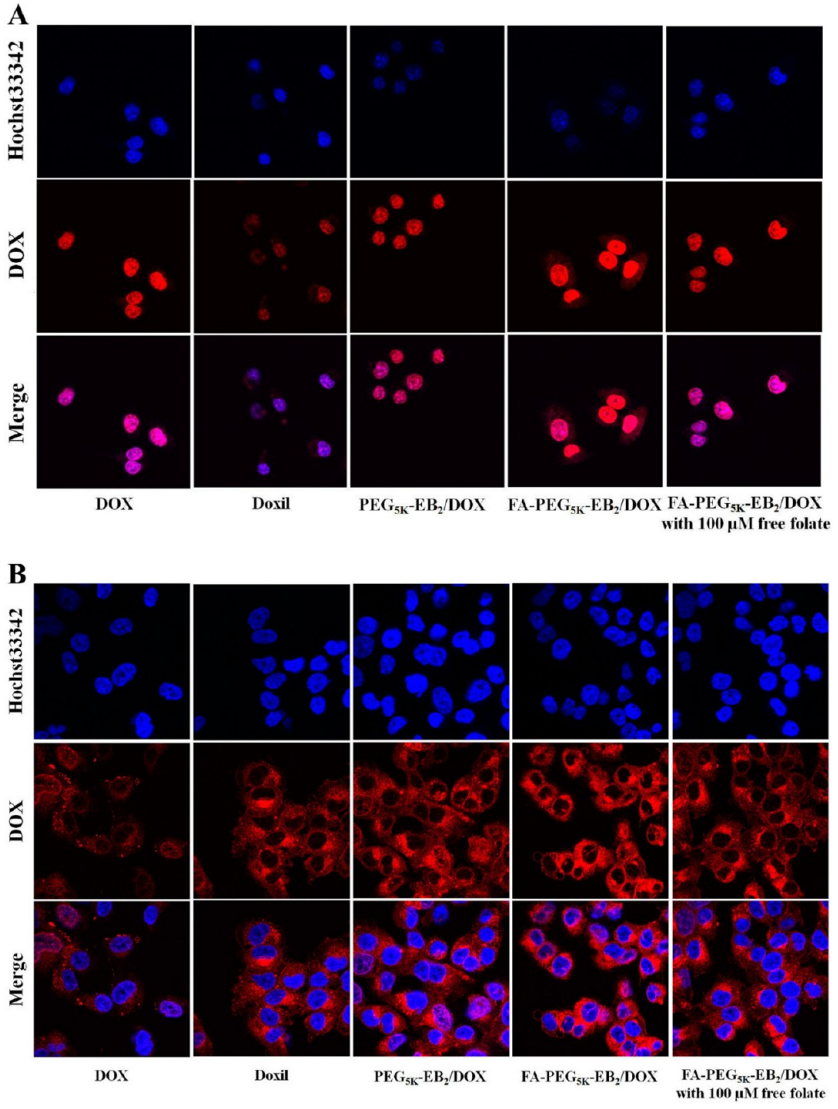

Figure 6. Confocal laser scanning microscopy (CLSM) images of 4T1.2 (A) and NCI/ADR-RES (B) cells after incubation with different DOX formulations for 30 min. DOX concentration was 6 μg/mL.

of DOX fluorescence intensity compared to free DOX-treated-NCI/ADR-RES cells (Figure 7B). These data are consistent with the cytotoxicity data and suggest that DOX formulated in PEG_{5K}-EB_2 micelles could be effectively taken up by cells and exerted its cytotoxic activity against the tumor cells. More importantly, the data suggest that DOX/PEG_{5K}-EB_2 could overcome the P-gp-mediated DOX efflux and resensitize NCI/ADR-RES cells to DOX cytotoxicity.

Inhibitory Effect of PEG_{5K}-EB_2 on P-gp ATPase. Despite the interesting observation that PEG_{5K}-EB_2 micelles were capable of reversing the DOX resistance in NCI/ADR-RES cells, the underlying mechanism remains unclear. It is possible that DOX formulated in PEG_{5K}-EB_2 micelles is taken up by an endocytosis pathway that renders the intracellularly delivered DOX less accessible to P-gp. We hypothesize that PEG_{5K}-EB_2 also overcomes the DOX resistance via directly inhibiting the activity of P-gp ATPase. It is well known that the activity of P-gp is energy-dependent. Thus, the hydrolysis of ATP by ATPase is a prerequisite to confer sufficient energy for the proper functionality of P-gp.[46] To confirm that PEG_{5K}-EB_2 is, indeed, a P-gp inhibitor, the effect of PEG_{5K}-EB_2 on P-gp activity was investigated via examining its inhibitory effect on verapamil-stimulated P-gp ATPase activity (Figure 8). TPGS was utilized as a positive control due to its known inhibitory effect on P-gp activity.[47] As shown in Figure 8, ΔRLU represents the consumption of ATP in the system. Consistent with previous reports, TPGS was able to significantly reduce the ΔRLU in a concentration-dependent manner, suggesting the potent inhibition on verapamil-stimulated P-gp ATPase activity, which can lead to the decreased activity of P-gp efflux pump. Interestingly, the ΔRLU in PEG_{5K}-EB_2 group also was significantly reduced, indicating the significant inhibitory effect of PEG_{5K}-EB_2 on P-gp ATPase activity. These data support our hypothesis that PEG_{5K}-EB_2 is able to reverse the P-gp-mediated multidrug resistance through blocking the function of P-gp. There are two possible mechanisms that are involved in the inhibition of P-gp ATPase by PEG_{5K}-EB_2. First, PEG_{5K}-EB_2 may bind to the ATPase-substrate complex to hinder the activity of ATPase so that ATP will not be hydrolyzed. Second, PEG_{5K}-EB_2 may be a substrate of ATPase and directly compete with other substrates for the binding of ATPase. More studies are underway to unravel how PEG_{5K}-EB_2 inhibits P-gp activity. It should be noted that other than DOX, there are many other potent chemotherapeutics that are the substrates of P-gp, such

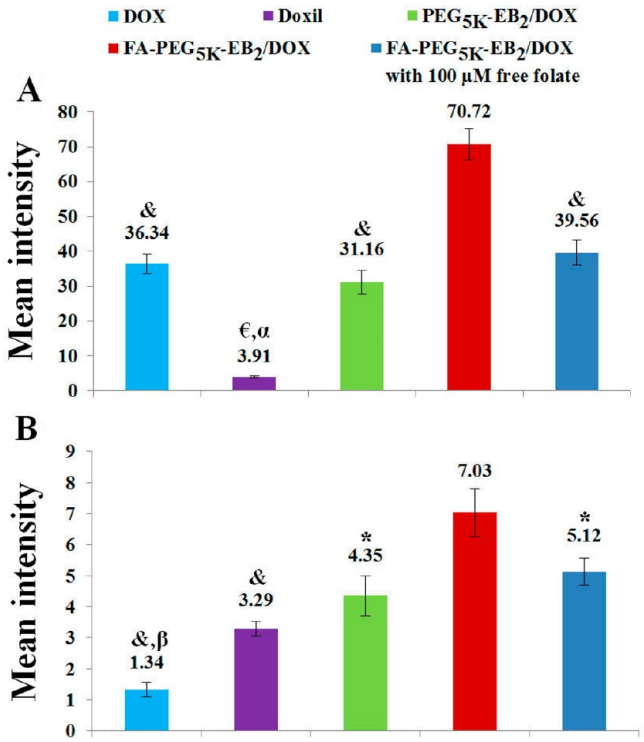

Figure 7. Cellular uptake of DOX in 4T1.2 (A) and NCI/ADR-RES (B) treated by DOX, Doxil, PEG_{5K}-EB_2/DOX, FA-PEG_{5K}-EB_2/DOX as well as FA-PEG_{5K}-EB_2/DOX with 100 μM free folate for 30 min. The numbers above each column are mean intensity values provided by the flow cytometry software, which represent the fluorescence intensity of the cells. Values are reported as the means ± SD for triplicate samples. DOX concentration was 6 μg/mL. $^{*}p < 0.05$, $^{\&}p < 0.005$, $^{€}p < 0.0001$, compared to FA-PEG_{5K}-EB_2/DOX. $^{\alpha}p < 0.0001$, $^{\beta}p < 0.005$ compared to PEG_{5K}-EB_2/DOX.

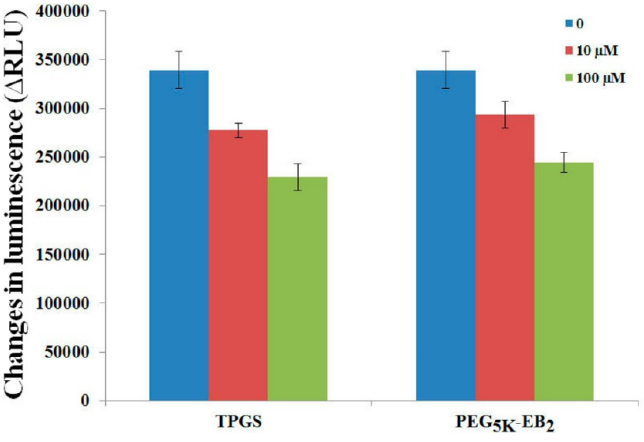

Figure 8. Inhibitory effect of PEG_{5K}-EB_2 and TPGS on verapamil-stimulated P-gp ATPase activity. Test samples containing verapamil (50 μM) and PEG_{5K}-EB_2 (10 or 100 μM) or Na_3VO_4 (a selective inhibitor of P-gp) were incubated with P-gp membrane for 5 min at 37 °C. Then the reaction was initiated by the addition of MgATP followed by another 40 min incubation at 37 °C. ATP detection reagent was then added followed by the examination of luminescence. Values are reported as the means ± SD for triplicate samples.

as paclitaxel, camptothecin, and etoposide. Therefore, our system can potentially be extended to delivery of these therapeutic agents to drug-resistant tumors.

Maximum Tolerated Dose (MTD) Study. One of the potential advantages of drug delivery via nanocarriers is the reduced systemic toxicity of the formulated drugs, which allows for increased dosage to be administered to maximize the therapeutic effect. To evaluate whether our DOX-loaded PEG_{5K}-EB_2 micelles could similarly reduce the DOX-related systemic toxicity, the MTD following a single iv administration of PEG_{5K}-EB_2/DOX micelles was investigated in tumor-free mice and compared to free DOX (Table 4). The mice were

Table 4. MTD of DOX and DOX-Loaded PEG_{5K}-EB_2: Micelles

formulations	dose (mg/kg)	animal death	weight loss (%)
Free DOX	5	0/3	2.2
	10	0/3	7.8
	15	2/3	N/A
DOX-loaded PEG_{5K}-EB_2 micelles	5	0/3	−2.5
	10	0/3	1.8
	15	0/3	6.9
	20	1/3	N/A
	30	3/3	N/A

treated with iv administration of different doses of DOX-loaded PEG_{5K}-EB_2 micelles or free DOX followed by observation of changes in body weight and other general signs of toxicity. As shown in Table 4, free DOX was well tolerated in mice at the dose of 10 mg DOX/kg. However, increasing the DOX dosage to 15 mg/kg caused the death of 2 out of 3 treated mice. Therefore, the MTD for free DOX at a single injection was around 10 mg/kg, which was consistent with published work.[48] In DOX-loaded PEG_{5K}-EB_2 micelles-treated mice, average weight loss was only 6.9% and there were no marked changes in the general activity at a DOX dosage of 15 mg/kg. Increasing the dosage to 20 mg DOX/kg led to the death of one out of 3 treated mice. Based on these data it was estimated that the single iv MTD for DOX-loaded PEG_{5K}-EB_2 micelles was 15 mg DOX/kg, which was a 1.5-fold improvement over free DOX. The improved MTD of DOX-loaded PEG_{5K}-EB_2 is likely attributed to multiple mechanisms. First, DOX-loaded PEG_{5K}-EB_2 showed slow and sustained release kinetics (Figure 3). Second, the PEG shielding of DOX-loaded PEG_{5K}-EB_2 micelles shall minimize the nonspecific uptake by major organs such as liver, heart, and lungs. Finally, embelin has hepatoprotective and anti-inflammatory activity,[49−51] which may counteract the adverse effects associated with DOX. More studies are needed to better understand the mechanism involved in the reduced toxicity of DOX-loaded PEG_{5K}-EB_2 micelles.

Near Infrared Fluorescence Imaging (NIRI) In Vivo and Ex Vivo. Previously, tumor-targeting effect of PEG_{5K}-EB_2 was examined in PC-3 xenograft tumor model, in which PEG_{5K}-EB_2 micelles coloaded with PTX and DiD were able to preferentially accumulate in the tumors. In this study, tumor-targeting ability of PEG_{5K}-EB_2 micelles was further investigated in nude mice bearing subcutaneous CL1 tumors by using DiR as a near-infrared fluorescence dye. DiR is a strong lipophilic tricarbocyanine probe and has longer excitation and emission wavelengths in the infrared range than DiD. In addition, it is able to prevent any light absorption by tissues, and avoid autofluorescence and scattering that are commonly associated with the application of visible light dyes.[52] Therefore, DiR is a useful NIRF dye for in vivo optical imaging. The mice injected

dx.doi.org/10.1021/mp500389v | Mol. Pharmaceutics 2014, 11, 4164−4178

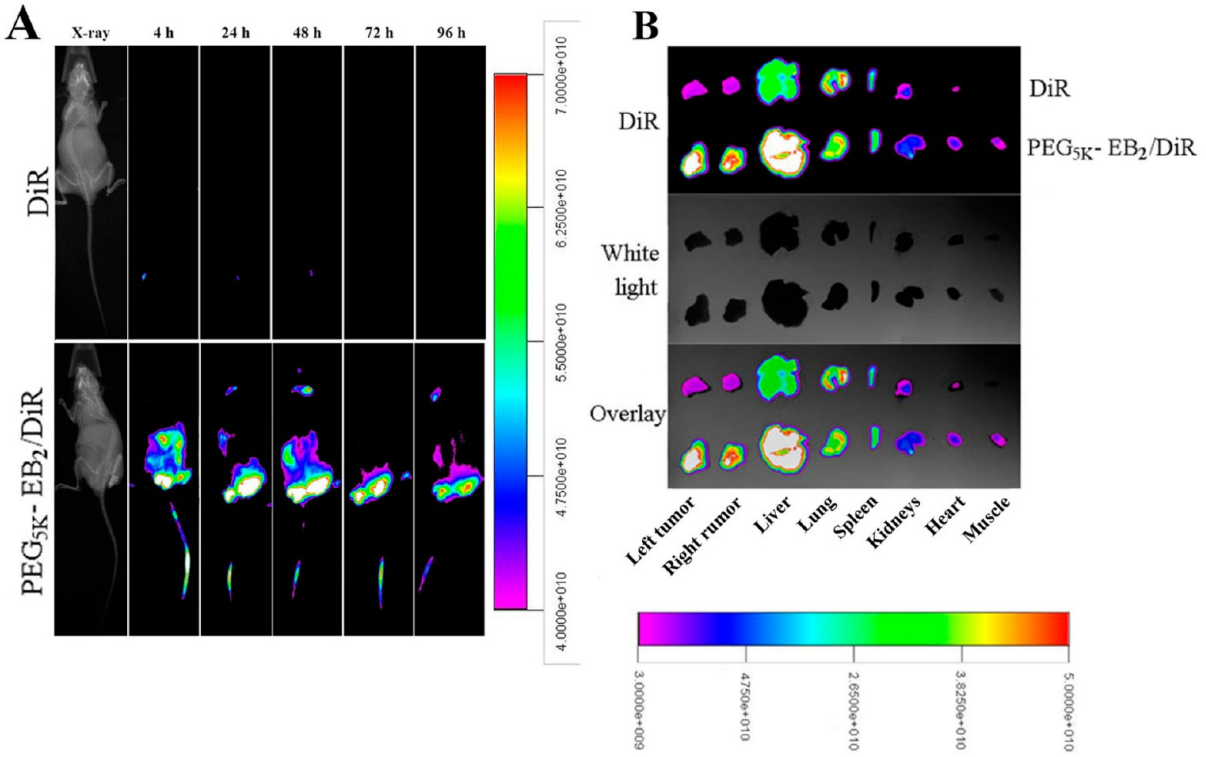

Figure 9. In vivo (A) and ex vivo (B) NIRF optical images of CL1 tumor-bearing SCID mice injected intravenously with free DiR dye and DiR-loaded PEG_{5K}-EB_2 micelles, respectively. Tumors and major organs were excised for ex vivo imaging at 96 h postinjection.

with free DiR showed no noticeable fluorescence signal in tumors and major organs throughout the 96 h period (Figure 9A). This may be mainly due to the rapid elimination of free DiR by RES and kidney.[53] In a sharp contrast, incorporation of DiR into PEG_{5K}-EB_2 micelles led to significantly enhanced accumulation of DiR at tumors. At 4 h post injection, an intense fluorescence signal was discerned in tumor areas, which peaked at 24 h and remained at a substantial level at 96 h, suggesting that PEG_{5K}-EB_2/DiR micelles were able to penetrate leaky tumor vasculature and retained in tumors throughout the 96 h period. This pronounced tumor distribution of DiR/PEG_{5K}-EB_2 micelles could be attributed to the nanosized particles by taking advantaging of EPR. Moreover, the strong interaction between DiR and embelin molecules may contribute to the excellent stability of the DiR/PEG_{5K}-EB_2 micelles prior to reaching the tumor tissues. More importantly, PEG corona in micelles further prevents the DiR from opsonization. Following the final imaging at 96 h postinjection, mice were sacrificed and tumors and major organs were excised, imaged, and quantified using a Carestream Molecular Imaging System. The intensity of the DiR signal varied in different organs. In free DiR-treated mouse, there was negligible signal of DiR observed in tumors. This is in contrast to the dramatically intense fluorescence signal in tumors for DiR-loaded PEG_{5K}-EB_2 micelles. Not surprisingly, moderate levels of fluorescence signal were observed in liver, spleen, and lungs as these are major organs that are accountable for the nonspecific clearance of alien particles by the RES. Table 5 showed the ratios of DiR signal intensity of tumor to that of liver or spleen. The ratios of tumor/liver in left and right tumors in PEG_{5K}-EB_2/DiR micelles were 5.44 and 5.27 folds higher than that for free DiR. Similar results were shown for tumor/spleen ratios. These data demonstrated that PEG_{5K}-EB_2 micelles are effective

Table 5. Ratios of DiR Signal Intensity of Tumor to Liver or Spleen

	tumor liver		tumor spleen	
	left tumor	right tumor	left tumor	right tumor
DiR	0.146	0.139	0.281	0.267
PEG_{5K}-EB_2 DiR	0.940	0.871	2.200	2.038

nanocarriers that are able to deliver anticancer therapeutics specifically to tumors.

Pharmacokinetics and Biodistribution. In vivo pharmacokinetic profile of DOX was investigated after iv bolus in BALB/c mice with the DOX concentration set at 5 mg/kg. Figure 10A compared the DOX blood clearance curves among three DOX formulations. The blood retention times of DOX in both DOX micellar formulations were significantly increased compared to free DOX. The pharmacokinetic parameters were obtained by fitting the blood DOX concentration versus time using a noncompartment model and summarized in Table 6. Incorporation of DOX into PEG_{5K}-EB_2 or FA-PEG_{5K}-EB_2 micelles led to substantially greater $t_{1/2}$, AUC, and C_{max} compared to free DOX. The $t_{1/2}$, AUC, and C_{max} of PEG_{5K}-EB_2/FA-PEG_{5K}-EB_2 were 1.76/2.47, 12.86/14.56, and 4.62/5.45-folds higher, respectively, than those of free DOX. However, V_d and CL for both micellar DOX formulations were significantly lower than those for free DOX. These data suggest that DOX formulated in PEG_{5K}-EB_2 or FA-PEG_{5K}-EB_2 micelles was well confined within the blood circulation with significantly increased half-life.

Next, we went to investigate whether our micellar formulations can improve the biodistribution of DOX. Free DOX, DOX-loaded PEG_{5K}-EB_2, and FA-PEG_{5K}-EB_2 micelles were iv administered to 4T1.2 tumor bearing mice at a DOX

dx.doi.org/10.1021/mp500389v | Mol. Pharmaceutics 2014, 11, 4164−4178

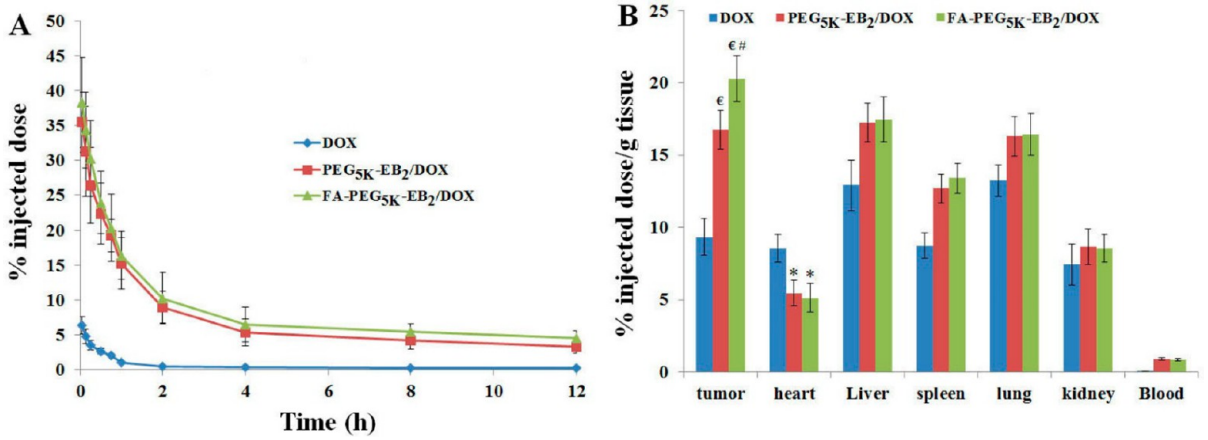

Figure 10. DOX pharmacokinetics (A) and biodistribution profiles (B) after intravenous administration in various DOX formulations at the dose of 5 mg/kg. Values are reported as the means ± SD for triplicate samples *p-value <0.05 compared to DOX, €p-value <0.005 compared to DOX, #p-value <0.05 compared to PEG_{5K}-EB_2/DOX.

Table 6. Pharmacokinetic Parameters of DOX in Different Formulations

	$t_{1/2}$ (h)	AUC (μg/mL × h)	CL (mL/h)	C_{max} (μg/mL)	V_d (mL)
DOX	4.41 ± 0.79	5.09 ± 0.31	19.71 ± 1.2	3.23 ± 0.19	26.73 ± 2.12
PEG_{5K}-EB_2/DOX	12.18 ± 1.25	70.54 ± 2.08	1.42 ± 0.042	18.14 ± 1.16	5.16 ± 0.49
FA-PEG_{5K}-EB_2/DOX	15.31 ± 0.94	79.18 ± 5.71	1.17 ± 0.22	20.84 ± 1.55	4.43 ± 0.40

concentration of 5 mg/kg. At 24 h after injection, tumors, blood, and major organs were collected for the measurement of DOX. Compared to free DOX, there were significantly greater amounts of DOX accumulation at tumors for DOX-loaded PEG_{5K}-EB_2 micelles (Figure 10B). This likely was attributed to the extended circulation time of DOX-loaded PEG_{5K}-EB_2 micelles and the EPR effect. Coupling of FA to the micellar DOX was associated with further improvement in tumor accumulation of DOX. Both FA-targeted and nontargeted micellar DOX are expected to extravasate into tumors due to their small sizes and the extended half-life in the blood circulation. However, surface decoration with FA shall facilitate the retention of the extravasated micellar DOX at tumor tissues via the FA/folate receptor interaction. FA can further facilitate the subsequent step of intracellular delivery following extravasation.

In addition to enhanced tumor accumulation, relatively high levels of DOX uptake were also noted in liver, spleen, and lungs, which could be ascribed to the nonspecific elimination of nanoparticles by RES. Interestingly, DOX distribution into the heart was significantly reduced in both DOX micellar formulations compared with free DOX. This is significant considering that cardiotoxicity is a major side effect that limits the amount of DOX that can be administered.

In Vivo Antitumor Activity. A highly metastatic breast cancer (4T1.2) model was selected in this study to assess the therapeutic efficacy of DOX-loaded micelles in comparison to free DOX and Doxil. An uncontrolled tumor growth was shown in the saline-treated group, which was consistent with the aggressive nature of the 4T1.2 tumor model. Mice treated with free DOX showed modest tumor growth inhibition compared to the saline group with an inhibition rate (IR) of 44.22% (Table 7). The PEGylated liposomal formulation of DOX, Doxil, exhibited improved antitumor activity over DOX (Figure 11A). The IR in the Doxil group was 66.97%, which is an improvement of approximately 1.5-fold over free DOX. The enhanced antitumor activity of Doxil over free DOX is likely

Table 7. Tumor Growth Inhibition Rate in Different Treatment Groups

treatments	IR (%)[a]
DOX	44.22
Doxil	66.97
PEG_{5K}-EB_2:DOX	78.18
FA-PEG_{5K}-EB_2:DOX	85.45

[a]Inhibition rate, IR (%) = (1 − relative tumor volume in the treated group/relative tumor volume in the saline group) × 100%

attributed to improved DOX accumulation at the tumor site due to the EPR effect.[3,4] Our data also showed that DOX-loaded PEG_{5K}-EB_2 micelles were even more effective than Doxil with an IR of 78.18% (Figure 11 and Table 7). Furthermore, addition of folic acid to the surface of the PEG_{5K}-EB_2/DOX micelles led to an additional improvement in antitumor activity with an IR of 85.45%. The further improvement of DOX-loaded PEG_{5K}-EB_2 micelles over Doxil is likely due to the very small size of PEG_{5K}-EB_2 micelles (~20 nm). It has been generally known that particles of <200 nm can effectively extravasate into solid tumors. However, recent studies have suggested that subnano-size (<100 nm) is critical for the particles to minimize the nonspecific uptake by liver and lungs and effectively penetrate the solid tumors including poorly vascularized tumors.[17,18] In addition to facilitating effective tumor accumulation, the inhibitory effect of PEG_{5K}-EB_2 on P-gp function may play a role in the improved antitumor activity of DOX-loaded PEG_{5K}-EB_2 micelles. Finally, the potential synergistic action between the embelin-based carrier and DOX may contribute to the overall antitumor activity. Figure 11B and 11D show the images and weights of the tumors collected at the completion of the experiment, which were in agreement with the tumor growth curves (Figure 11A). During the entire period of the in vivo study, there were no noticeable body weight changes in all treatment groups compared to the saline group (Figure 11C). Additionally, serum levels of trans-

dx.doi.org/10.1021/mp500389v | Mol. Pharmaceutics 2014, 11, 4164−4178

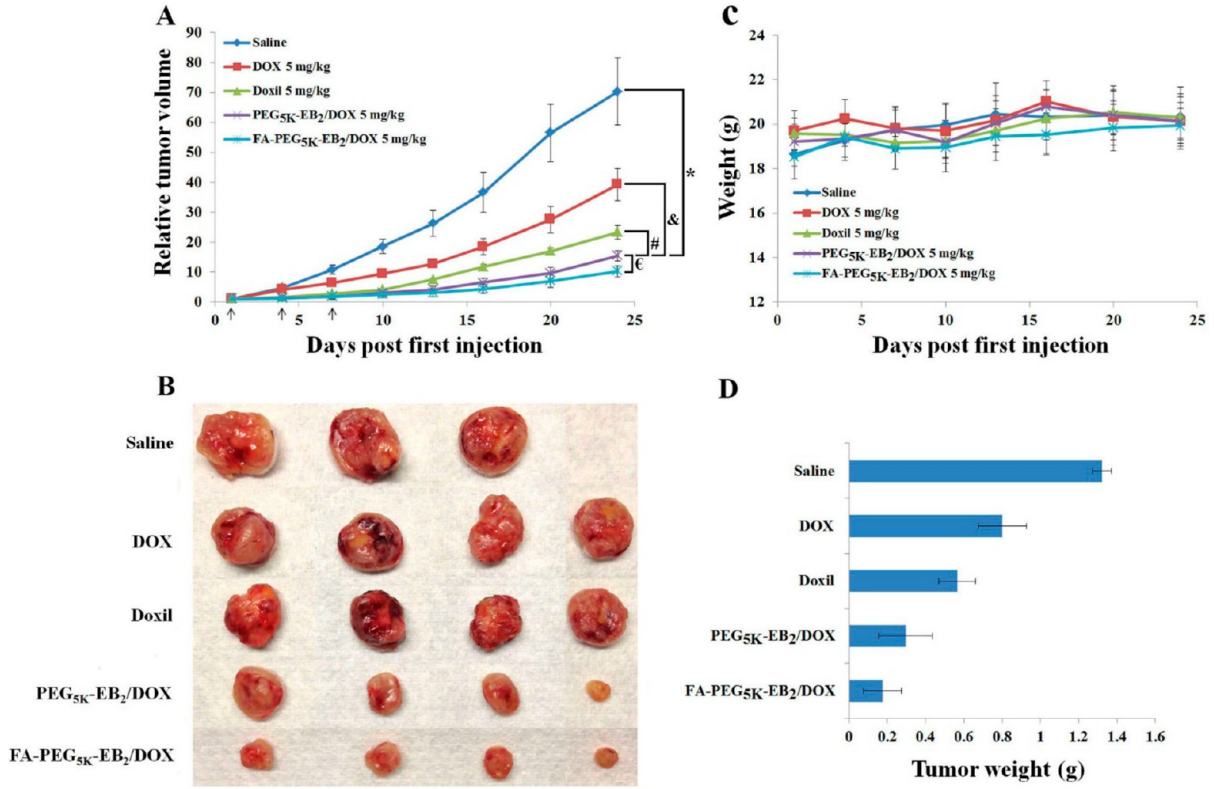

Figure 11. In vivo therapeutic study of different DOX formulations in 4T1.2 syngeneic mouse model. Solid arrows mean the iv administration. A: relative tumor volume. B: body weight. *p-value (PEG_{5K}-EB_2/DOX vs Saline) < 0.0001. &p-value (PEG_{5K}-EB_2/DOX vs DOX·HCl) < 0.001. #p-value (PEG_{5K}-EB_2/DOX vs Doxil) < 0.01. €p-value (PEG_{5K}-EB_2/DOX vs FA- PEG_{5K}-EB_2/DOX) < 0.05.

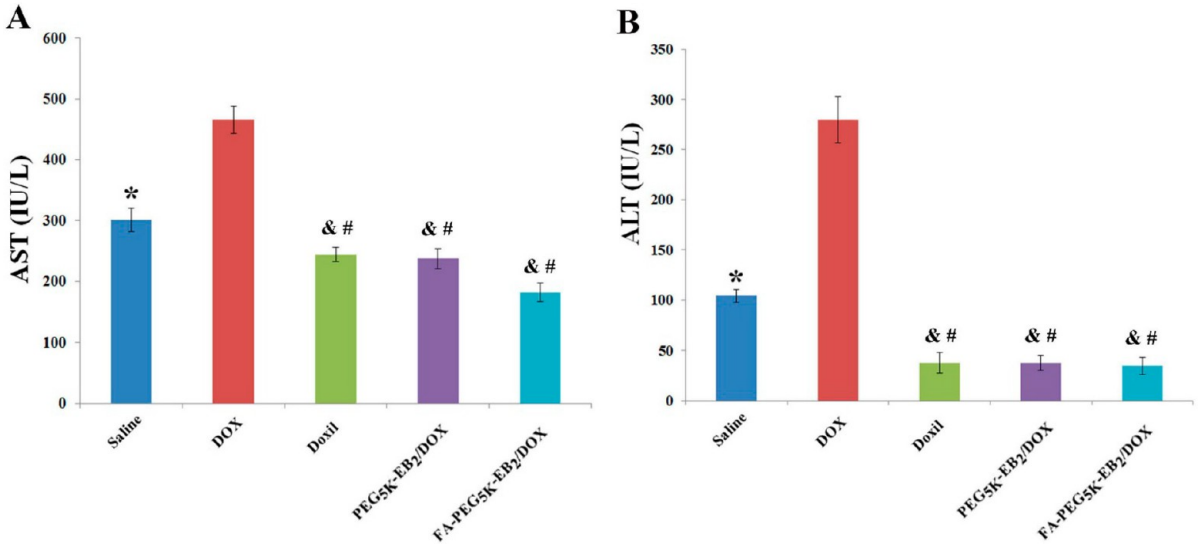

Figure 12. Aspartate aminotransferase (AST) and alanine aminotransferase (ALT) level in different DOX formulations. *p-value <0.05, compared to DOX, #p-value <0.01, compared to DOX, &p-value <0.05, compared to saline.

aminases (AST and ALT) in the mice from all groups were examined (Figure 12). The AST and ALT levels in the DOX-treated group were significantly higher than those in the saline-treated group, suggesting a DOX-related toxicity. No increases in serum levels of AST and ALT were found in the mice treated with Doxil or the DOX-loaded PEG_{5K}-EB_2 micelles. Our data suggest that incorporation of DOX into PEG_{5K}-EB_2 micellar formulation can lead to significantly improved antitumor activity with minimal toxicity.

CONCLUSIONS

In this study, folic acid-targeted PEG_{5K}-EB_2 (FA-PEG_{5K}-EB_2) nanoassembly was successfully developed and utilized as a multifunctional carrier to formulate DOX. Our data show that FA-PEG_{5K}-EB_2 micelles can efficiently load DOX and form stable and spherical nanoassemblies with a size around 20 nm. DOX formulated in FA-PEG_{5K}-EB_2 micelles exhibited slow and controlled release kinetics, which should provide improved

dx.doi.org/10.1021/mp500389v | Mol. Pharmaceutics 2014, 11, 4164−4178

stability in the blood and sustained action upon reaching the tumor. Cellular uptake studies showed enhanced intracellular delivery with DOX-loaded, FA-decorated PEG_{5K}-EB_2 system, which correlated with improved cytotoxicity in vitro. More importantly, PEG_{5K}-EB_2 micelles were able to effectively reverse the multidrug resistance by interfering with the function of P-gp, contributing to the increased intracellular delivery of the loaded drugs. In vivo MTD studies demonstrated that DOX-loaded PEG_{5K}-EB_2 micelles had a better safety profile than free DOX. In addition, PEG_{5K}-EB_2/DOX formulations displayed significantly longer blood residence time and greater uptake in tumors than free DOX with significantly less heart distribution. Finally, superior antitumor activity in PEG_{5K}-EB_2/DOX micelles was achieved over DOX and Doxil in a 4T1.2 breast cancer model. The attachment of FA to the PEG_{5K}-EB_2/DOX micelles led to an additional improvement in tumor growth inhibition. Our data suggest that the multifunctional FA-PEG_{5K}-EB_2 nanomicelles hold promise as a safe and effective drug carrier, which merits further study in the future.

■ ASSOCIATED CONTENT

Supporting Information

HPLC trace, ^{1}H NMR, and MALDI−TOF of FA-$PEG_{7.5K}$-DOA. This material is available free of charge via the Internet at http://pubs.acs.org/

■ AUTHOR INFORMATION

Corresponding Author

*E-mail: sol4@pitt.edu. Tel: 412-383-7976 Fax: 412-648-1664. Address: Center for Pharmacogenetics, University of Pittsburgh School of Pharmacy, 639 Salk Hall, Pittsburgh, Pennsylvania 15261, United States.

Notes

The authors declare no competing financial interest.

■ ACKNOWLEDGMENTS

This work was supported in part by NIH grants RO1CA174305, R01GM102989, and R21CA173887.

■ REFERENCES

(1) Takemura, G.; Fujiwara, H. Doxorubicin-induced cardiomyopathy from the cardiotoxic mechanisms to management. *Prog. Cardiovasc. Dis.* **2007**, *49*, 330−352.

(2) Minotti, G.; Menna, P.; Salvatorelli, E.; Cairo, G.; Gianni, L. Anthracyclines: molecular advances and pharmacologic developments in antitumor activity and cardiotoxicity. *Pharmacol. Rev.* **2004**, *56*, 185−229.

(3) Matsumura, Y.; Maeda, H. A new concept for macromolecular therapeutics in cancer chemotherapy: mechanism of tumoritropic accumulation of proteins and the antitumor agent smancs. *Cancer Res.* **1986**, *46*, 6387−6392.

(4) Gao, Z.; Lukyanov, A. N.; Singhal, A.; Torchilin, V. P. Diacyllipid-Polymer Micelles as Nanocarriers for Poorly Soluble Anticancer Drugs. *Nano Lett.* **2002**, *2*, 979−982.

(5) Li, S. D.; Huang, L. Nanoparticles evading the reticuloendothelial system: role of the supported bilayer. *Biochim. Biophys. Acta* **2009**, *1788*, 2259−2266.

(6) Woodle, M. C.; Engbers, C. M.; Zalipsky, S. New amphipatic polymer-lipid conjugates forming long-circulating reticuloendothelial system-evading liposomes. *Bioconjugate Chem.* **1994**, *5*, 493−496.

(7) O'Brien, M. E.; Wigler, N.; Inbar, M.; Rosso, R.; Grischke, E.; Santoro, A.; Catane, R.; Kieback, D. G.; Tomczak, P.; Ackland, S. P.; Orlandi, F.; Mellars, L.; Alland, L.; Tendler, C. CAELYX Breast Cancer Study Group. Reduced cardiotoxicity and comparable efficacy in a phase III trial of pegylated liposomal doxorubicin HCl (CAELYX/Doxil) versus conventional doxorubicin for first-line treatment of metastatic breast cancer. *Ann. Oncol.* **2004**, *15*, 440−449.

(8) Al-Batran, S. E.; Meerpohl, H. G.; Von Minckwitz, G.; Atmaca, A.; Kleeberg, U.; Harbeck, N.; Lerbs, W.; Hecker, D.; Sehouli, J.; Knuth, A.; Jager, E. Reduced incidence of severe palmar-plantar erythrodysesthesia and mucositis in a prospective multicenter phase II trial with pegylated liposomal doxorubicin at 40 mg/m2 every 4 weeks in previously treated patients with metastatic breast cancer. *Oncology* **2006**, *70*, 141−146.

(9) Lorusso, D.; Di Stefano, A.; Carone, V.; Fagotti, A.; Pisconti, S.; Scambia, G. Pegylated liposomal doxorubicin-related palmar-plantar erythrodysesthesia ("hand−foot" syndrome). *Ann. Oncol.* **2007**, *18*, 1159−1164.

(10) Von Gruenigen, V.; Frasure, H.; Fusco, N.; DeBernardo, R.; Eldermire, E.; Eaton, S.; Waggoner, S. A double-blind, randomized trial of pyridoxine versus placebo for the prevention of pegylated liposomal doxorubicin-related hand−foot syndrome in gynecologic oncology patients. *Cancer* **2010**, *116*, 4735−4743.

(11) Sutton, D.; Nasongkla, N.; Blanco, E.; Gao. Functionalized micellar systems for cancer targeted drug delivery. *J. Pharm. Res.* **2007**, *24*, 1029−1046.

(12) Huang, Y.; Lu, J.; Gao, X.; Li, J.; Zhao, W.; Sun, M.; Stolz, D. B.; Venkataramanan, R.; Rohan, L. C.; Li, S. PEG-derivatized embelin as a dual functional carrier for the delivery of paclitaxel. *Bioconjugate Chem.* **2012**, *23*, 1443−1451.

(13) Lu, J.; Huang, Y.; Zhao, W.; Marquez, R. T.; Meng, X.; Li, J.; Gao, X.; Venkataramanan, R.; Wang, Z.; Li, S. PEG-derivatized embelin as a nanomicellar carrier for delivery of paclitaxel to breast and prostate cancers. *Biomaterials* **2013**, *34*, 1591−1600.

(14) Lu, J.; Huang, Y.; Zhao, W.; Chen, Y.; Li, J.; Gao, X.; Venkataramanan, R.; Li, S. Design and characterization of PEG-derivatized vitamin E as a nanomicellar formulation for delivery of paclitaxel. *Mol. Pharmaceutics* **2013**, *10*, 2880−2890.

(15) Zhang, X.; Lu, J.; Huang, Y.; Zhao, W.; Chen, Y.; Li, J.; Gao, X.; Venkataramanan, R.; Sun, M.; Stolz, D. B.; Zhang, L.; Li, S. PEG-farnesylthiosalicylate conjugate as a nanomicellar carrier for delivery of paclitaxel. *Bioconjugate Chem.* **2013**, *24*, 464−472.

(16) Gao, X.; Huang, Y.; Makhov, A. M.; Epperly, M.; Lu, J.; Grab, S.; Zhang, P.; Rohan, L.; Xie, X. Q.; Wipf, P.; Greenberger, J.; Li, S. Nanoassembly of surfactants with interfacial drug-interactive motifs as tailor-designed drug carriers. *Mol. Pharmaceutics* **2013**, *10*, 187−198.

(17) Luo, J.; Xiao, K.; Li, Y.; Lee, J. S.; Shi, L.; Tan, Y. H.; Xing, L.; Holland Cheng, R.; Liu, G. Y.; Lam, K. S. Well-defined, size-tunable, multifunctional micelles for efficient paclitaxel delivery for cancer treatment. *Bioconjugate Chem.* **2010**, *21*, 1216−1224.

(18) Li, Y.; Xiao, K.; Luo, J.; Lee, J.; Pan, S.; Lam, K. S. A novel size-tunable nanocarrier system for targeted anticancer drug delivery. *J. Controlled Release* **2010**, *144*, 314−323.

(19) Bedi, D.; Gillespie, J. W.; Petrenko, V. A., Jr.; Ebner, A.; Leitner, M.; Hinterdorfer, P.; Petrenko, V. A. Targeted delivery of siRNA into breast cancer cells via phage fusion proteins. *Mol. Pharmaceutics* **2013**, *10*, 551−559.

(20) Cheng, C.; Wei, H.; Zhu, J. L.; Chang, C.; Cheng, H.; Li, C.; Cheng, S. X.; Zhang, X. Z.; Zhuo, R. X. Functionalized thermoresponsive micelles self-assembled from biotin-PEG-b-P(NIPAAm-co-HMAAm)-b-PMMA for tumor cell target. *Bioconjugate Chem.* **2008**, *6*, 1194−1201.

(21) Song, N.; Ding, M.; Pan, Z.; Li, J.; Zhou, L.; Tan, H.; Fu, Q. Construction of targeting-clickable and tumor-cleavable polyurethane nanomicelles for multifunctional intracellular drug delivery. *Biomacromolecules* **2013**, *14*, 4407−4419.

(22) Wang, T.; Petrenko, V. A.; Torchilin, V. P. Paclitaxel-loaded polymeric micelles modified with MCF-7 cell-specific phage protein: enhanced binding to target cancer cells and increased cytotoxicity. *Mol. Pharmaceutics* **2010**, *7*, 1007−1014.

(23) Lächelt, U.; Wittmann, V.; Müller, K.; Edinger, D.; Kos, P.; Höhn, M.; Wagner, E. Synthetic Polyglutamylation of Dual-Functional

MTX Ligands for Enhanced Combined Cytotoxicity of Poly(I:C) Nanoplexes. *Mol. Pharm.* **2014**, No. 10.1021/mp500017u.
(24) Yan, L.; Chen, W.; Zhu, X.; Huang, L.; Wang, Z.; Zhu, G.; Roy, V. A.; Yu, K. N.; Chen, X. Folic acid conjugated self-assembled layered double hydroxide nanoparticles for high-efficacy-targeted drug delivery. *Chem. Commun. (Cambridge)* **2013**, *49*, 10938−10940.
(25) Li, H.; Piao, L.; Yu, B.; Yung, B. C.; Zhang, W.; Wang, P. G.; Lee, J. L.; Lee, R. J. Delivery of calf thymus DNA to tumor by folate receptor targeted cationic liposomes. Delivery of calf thymus DNA to tumor by folate receptor targeted cationic liposomes. *Biomaterials* **2011**, *32*, 6614−6620.
(26) van Dongen, M. A.; Silpe, J. E.; Dougherty, C. A.; Kanduluru, A. K.; Choi, S. K.; Orr, B. G.; Low, P. S.; Banaszak Holl, M. M. Avidity mechanism of dendrimer-folic Acid conjugates. *Mol. Pharmaceutics* **2014**, *11*, 1696−1706.
(27) Danquah, M.; Li, F.; Duke, C. B.; Miller, D. D.; Mahato, R. I. Micellar delivery of bicalutamide and embelin for treating prostate cancer. *Pharm. Res.* **2009**, *26*, 2081−2092.
(28) Sreepriya, M.; Bali, G. Chemopreventive effects of embelin and curcumin against N-nitrosodiethylamine/phenobarbital-induced hepatocarcinogenesis in Wistar rats. *Fitoterapia* **2005**, *76*, 549−555.
(29) Dai, Y.; Qiao, L.; Chan, K. W.; Yang, M.; Ye, J.; Ma, J.; Zou, B.; Gu, Q.; Wang, J.; Pang, R.; Lan, H. Y.; Wong, B. C. Peroxisome proliferator-activated receptor-gamma contributes to the inhibitory effects of Embelin on colon carcinogenesis. *Cancer Res.* **2009**, *69*, 4776−4783.
(30) Heo, J. Y.; Kim, H. J.; Kim, S. M.; Park, K. R.; Park, S. Y.; Kim, S. W.; Nam, D.; Jang, H. J.; Lee, S. G.; Ahn, K. S.; Kim, S. H.; Shim, B. S.; Choi, S. H.; Ahn, K. S. Embelin suppresses STAT3 signaling, proliferation, and survival of multiple myeloma via the protein tyrosine phosphatase PTEN. *Cancer Lett.* **2011**, *308*, 71−80.
(31) Nikolovska-Coleska, Z.; Xu, L.; Hu, Z.; Tomita, Y.; Li, P.; Roller, P. P.; Wang, R.; Fang, X.; Guo, R.; Zhang, M.; Lippman, M. E.; Yang, D.; Wang, S. Discovery of embelin as a cell-permeable, small-molecular weight inhibitor of XIAP through structure-based computational screening of a traditional herbal medicine three-dimensional structure database. *J. Med. Chem.* **2004**, *47*, 2430−2440.
(32) Li, F.; Danquah, M.; Mahato, R. I. Synthesis and characterization of amphiphilic lipopolymers for micellar drug delivery. *Biomacromolecules* **2010**, *11*, 2610−2620.
(33) Zhang, Y.; Huang, Y.; Zhang, P.; Gao, X.; Gibbs, R. B.; Li, S. Incorporation of a selective sigma-2 receptor ligand enhances uptake of liposomes by multiple cancer cells. *Int. J. Nanomedicine* **2012**, *7*, 4473−4485.
(34) Paulos, C. M.; Reddy, J. A.; Leamon, C. P.; Turk, M. J.; Low, P. S. Ligand binding and kinetics of folate receptor recycling in vivo: impact on receptor-mediated drug delivery. *Mol. Pharmacol.* **2004**, *66*, 1406−1414.
(35) Wang, Y.; Wang, R.; Lu, X.; Lu, W.; Zhang, C.; Liang, W. Pegylated phospholipids-based self-assembly with water-soluble drugs. *Pharm. Res.* **2010**, *27*, 361−370.
(36) Hu, C. M.; Zhang, L. Therapeutic nanoparticles to combat cancer drug resistance. *Curr. Drug Metab.* **2009**, *10*, 836−841.
(37) Gottesman, M. M. Mechanisms of cancer drug resistance. *Annu. Rev. Med.* **2002**, *53*, 615−627.
(38) Yuan, H.; Li, X.; Wu, J.; Li, J.; Qu, X.; Xu, W.; Tang, W. Strategies to overcome or circumvent P-glycoprotein mediated multidrug resistance. *Curr. Med. Chem.* **2008**, *15*, 470−476.
(39) Chavanpatil, M. D.; Khdair, A.; Gerard, B.; Bachmeier, C.; Miller, D. W.; Shekhar, M. P.; Panyam, J. Surfactant-polymer nanoparticles overcome P-glycoprotein-mediated drug efflux. *Mol. Pharmaceutics* **2007**, *4*, 730−738.
(40) Collnot, E. M.; Baldes, C.; Wempe, M. F.; Kappl, R.; Hüttermann, J.; Hyatt, J. A.; Edgar, K. J.; Schaefer, U. F.; Lehr, C. M. Mechanism of inhibition of P-glycoprotein mediated efflux by vitamin E TPGS: influence on ATPase activity and membrane fluidity. *Mol. Pharmaceutics* **2007**, *4*, 465−474.
(41) Sharma, A. K.; Zhang, L.; Li, S.; Kelly, D. L.; Alakhov, V. Y.; Batrakova, E. V.; Kabanov, A. V. Prevention of MDR development in leukemia cells by micelle-forming polymeric surfactant. *J. Controlled Release* **2008**, *131*, 220−227.
(42) Zhang, Z.; Liu, Z.; Ma, L.; Jiang, S.; Wang, Y.; Yu, H.; Yin, Q.; Cui, J.; Li, Y. Reversal of multidrug resistance by mitochondrial targeted self-assembled nanocarrier based on stearylamine. *Mol. Pharmaceutics* **2013**, *10*, 2426−2434.
(43) Loo, T. W.; Bartlett, M. C.; Clarke, D. M. Disulfiram metabolites permanently inactivate the human multidrug resistance P-glycoprotein. *Mol. Pharmaceutics* **2004**, *1*, 426−433.
(44) Desai, P. V.; Sawada, G. A.; Watson, I. A.; Raub, T. J. Integration of in silico and in vitro tools for scaffold optimization during drug discovery: predicting P-glycoprotein efflux. *Mol. Pharmaceutics* **2013**, *10*, 1249−1261.
(45) Ogawara, K.; Un, K.; Tanaka, K.; Higaki, K. T. In vivo anti-tumor effect of PEG liposomal doxorubicin (DOX) in DOX-resistant tumor-bearing mice: Involvement of cytotoxic effect on vascular endothelial cells. *J. Controlled Release* **2009**, *133*, 4−10.
(46) Klaassen, C. D.; Aleksunes, L. M. Xenobiotic, bile acid, and cholesterol transporters: function and regulation. *Pharmacol. Rev.* **2010**, *62*, 1−96.
(47) Dintaman, J. M.; Silverman, J. A. Inhibition of P-glycoprotein by D-alpha-tocopheryl polyethylene glycol 1000 succinate (TPGS). *Pharm. Res.* **1999**, *16*, 1550−1556.
(48) Xiao, K.; Luo, J.; Li, Y.; Lee, J. S.; Fung, G.; Lam, K. S. PEG-oligocholic acid telodendrimer micelles for the targeted delivery of doxorubicin to B-cell lymphoma. *J. Controlled Release* **2011**, *155*, 272−281.
(49) Chitra, M.; Sukumar, E.; Suja, V.; Devi, C. S. Antitumor, anti-inflammatory and analgesic property of embelin, a plant product. *Chemotherapy* **1994**, *40*, 109−113.
(50) Bhandari, U.; Jain, N.; Pillai, K. K. Further studies on antioxidant potential and protection of pancreatic beta-cells by Embelia ribes in experimental diabetes. *Exp. Diabetes Res.* **2007**, *2007*, 15803−15808.
(51) Singh, D.; Singh, R.; Singh, P.; Gupta, R. S. Effects of embelin on lipid peroxidation and free radical scavenging activity against liver damage in rats. *Basic Clin. Pharmacol. Toxicol.* **2009**, *105*, 243−248.
(52) Chen, J.; Corbin, I. R.; Li, H.; Cao, W.; Glickson, J. D.; Zheng, G. Ligand conjugated low-density lipoprotein nanoparticles for enhanced optical cancer imaging in vivo. *J. Am. Chem. Soc.* **2007**, *129*, 5798−5799.
(53) Hou, L.; Yao, J.; Zhou, J.; Zhang, Q. Pharmacokinetics of a paclitaxel-loaded low molecular weight heparin-all-trans-retinoid acid conjugate ternary nanoparticulate drug delivery system. *Biomaterials* **2012**, *33*, 5431−5440.